ACS OMEGA

http://pubs.acs.org/journal/acsodf

Article

Influence of Quenching on the Opto-Electronic Properties of F:SnO_2 Layers

Laura Maria Manceriu,* Anthony Maho, Christine Labrugere, Eric Tixhon, Audrey Schrijnemakers, Aline Rougier, Pierre Colson, and Rudi Cloots*

Cite This: *ACS Omega* 2020, 5, 14999−15006

Read Online

ACCESS | Metrics & More | Article Recommendations | Supporting Information

ABSTRACT: For many opto-electronic applications, F:SnO_2 materials must benefit from high transparency, high conductivity, and high mechanical strength even after quenching. The purpose of this study was to investigate the influence of quenching on the opto-electronic properties of the F:SnO_2 layers synthesized at high temperature on Si_xC_yO-coated soda-lime glass by atmospheric chemical vapor deposition. The morphology, structure, and composition of the layers were studied before and after quenching in air- and oxygen-rich atmospheres at 670 °C. The free carrier concentration was reduced by oxygen vacancy (V_O) passivation, as well as by F and Na diffusion, with all effects scaling up with quenching time in air. The transmittance also decreased with quenching time as Na impurities acted as absorption and electron recombination centers. In an oxygen-rich atmosphere, the V_O passivation was even more emphasized, with however a moderate contribution to conductivity loss. The F:SnO_2 layer microstructure and composition were rather fringed through high-temperature deposition. The almost invariable free carrier concentration and transmittance of the F:SnO_2 samples quenched in O_2 versus air were related to a moderation in Na diffusion. For long quenching times (>20 min) in air, Na and F diffusion prevailed explaining the conductivity drop.

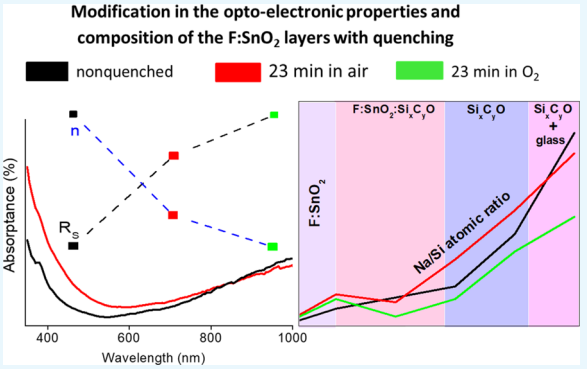

1. INTRODUCTION

Transparent conducting layers (TCLs) are essential components not only in solar energy conversion or solar control glazing applications, acting as buffer or collector layers,[1−4] but also in other (opto)electronic applications such as flat panel displays[5] or gas sensors.[6] The most popular TCLs are the doped metal oxides such as ITO (Sn:In_2O_3), AZO (Al:ZnO), and FTO (F:SnO_2). Particularly, FTO can be produced at low cost, having high mechanical, chemical, and electrochemical stability.[7]

Pristine SnO_2 is an n-type semiconductor with a wide optical band gap (E_g = 3.7 eV) and consequently high optical transparency (T > 85%).[8] In undoped SnO_2, the oxygen vacancies and interstitial Sn are the primary donor defects,[9] and consequently, Sn vacancies are present as well (eqs 1 and 2)[a]. Because the Sn_i^{4+} defects are localized in the conduction band and are fully ionized, it is widely accepted that the n-type conducting behavior is controlled by the oxygen vacancies ionization. This material electrical conductivity is usually enhanced by substitutional doping with fluorine (eq 3), reaching resistivity values as low as 10^{-3} Ω cm with charge mobilities of 20 $cm^2/(V\ s)$.[10] When fluorine is integrated in the network, it also fills up part of the oxygen vacancies (eq 4).

$$0 = 2V_O^{\bullet\bullet} + V_{Sn}^{4-} \quad (1)$$

$$0 = V_{Sn}^{4-} + Sn_i^{4+} \quad (2)$$

$$O_0^x + F_0^x \rightarrow F_O^{\bullet\bullet} + 1/2O_i'' \quad (3)$$

$$F_0^x + V_O^x + 3e^- \rightarrow F_O^{\bullet} + V_{Sn}^{4-} \quad (4)$$

High-quality FTO thin films are generally produced at a large industrial scale by high-temperature spray pyrolysis[11] or (atmospheric) chemical vapor deposition.[12] In the case of the latter process, F and Sn precursors are fed together in the chamber, their concentrations being separately controlled by gas flow before mixing. The film deposition occurs by vaporization, aerosol migration toward the heated substrate, condensation, and precursor pyrolysis.

In the specific context of glass industrial processing, quenching is the process of heat treatment for few minutes

Received: February 10, 2020
Accepted: June 5, 2020
Published: June 19, 2020

https://dx.doi.org/10.1021/acsomega.0c00589
ACS Omega 2020, 5, 14999−15006

at a temperature close to the glass softening point, $T \approx 650$ °C, followed by rapid cooling treatment so as to "freeze" the glass in a specific mechanical state—higher surface compression and/or edge compression—and composition.[13] The quenching process is imposed through several European standards (ASTM C1048, CPSC 16 CFR 1201, or ANSI Z97.1) for decorative, automotive, photovoltaic, or architectural glazing applications.

For most of the applications, including TCLs, soda-lime glass is used as the substrate because of its lower price. However, in the case of self-cleaning glass, it was already proven that Na diffusion from glass into the functional layer during post-deposition annealing treatments damages the self-cleaning property.[14] The TCLs' emissivity[15] and transparency[16] were also proven to be impacted by quenching. Investigating and improving the stability of TCLs toward quenching are therefore of high interest.

On the one hand, the modification of optical and electrical properties as function of annealing temperature and time was largely studied for F:SnO_2 samples synthesized at room[17] or moderate (400−450 °C)[16,18,19] temperatures using chemical or physical methods. These films usually suffer from major structural and morphological changes that engender the modification of the opto-electronic properties when annealed at $T > 450$ °C.

On the other hand, the behavior toward quenching of—highly crystalline—F:SnO_2 films deposited at high temperatures (500−600 °C) by industrial processes such as chemical vapor deposition was far less studied. Indeed, a Si_xC_yO barrier layer was incorporated to block Na diffusion from glass without damaging the glass final appearance. When using a 20 nm thick Si_xC_yO barrier layer, Gao et al.[20] showed that the grain size of F:SnO_2 films synthesized by atmosphere pressure chemical vapor deposition (APCVD) at 600 °C was reduced after quenching at $T > 580$ °C for 20 min. The structural stability of the same F:SnO_2 layers is improved by using a thicker barrier layer (70 nm of Si_xC_yO), showing that no crystallinity or morphological changes were observed for short annealing periods (20 min) at 650 °C. In both cases, the conductivity loss was explained through the grain boundary scattering mechanism with increasing quenching time. Na diffusion was also considered as a potential explanation but without any clear demonstration. The same study also concluded that the infrared reflectance decreased along with carrier concentration diminution.

On the contrary, Wang et al.[21,22] proved by using ellipsometry that the Na ions diffused into the barrier layer after quenching up to 120 min at 600 °C, as confirmed by the consequent transmission drop. In another study, Yang et al.[23] reported no change in the structural and morphological characteristics of F:SnO_2 layers deposited at 500 °C by APCVD after short time annealing (3−4 min) at 700 °C in air and explained the conductivity loss by the oxygen vacancy passivation mechanism. Again, Na diffusion was mentioned without any evidence to consequential conductivity drop. Oxygen vacancy passivation was also considered responsible for the conductivity drop of F:SnO_2 films deposited on the Si_xC_yO pre-coated glass after quenching at 600 °C for more than 10 min.[24] The same study highlighted some modifications in the structure and morphology of the layers, as well as the drop in transmittance in the visible region. The origin of optical changes was not further discussed. According to Akkad and Joseph,[18] the oxygen vacancies have a short diffusion length (20−26 Å); therefore, their passivation during cooling in air does not constitute the main cause for the carrier concentration decrease as this effect should be limited at the extreme surface of the FTO layer.

To conclude, there is a clear lack in understanding the impact of quenching on F:SnO_2-coated glass. Indeed, the relevant literature provides limited and sometimes contradictory insights into the film composition and structural and opto-electronic modifications with quenching.

The purpose of our study is to investigate the quenching-induced damaging of the opto-electronic properties of F:SnO_2 layers deposited by APCVD on the Si_xC_yO-coated glass in relation to microstructural and composition changes. Hence, the F:SnO_2 films were examined before and after quenching in normal (air) and oxygen-rich atmospheres. To our knowledge, no report can be found on APCVD-prepared F:SnO_2/Si_xC_yO layers quenched in the oxygen-rich atmosphere, neither on the simultaneous correlation of the composition with the opto-electronic properties. Moreover, the stability toward quenching of a Si_xC_yO barrier layer is here investigated for the first time.

2. RESULTS AND DISCUSSION

First, the electrical properties of the F:SnO_2 films were characterized for the nonquenched samples and after quenching in air at 670 °C for 6, 10, 15, and 23 min. The F:SnO_2 films were deposited on the Si_xC_yO-coated (~70 nm thick) soda-lime glass by APCVD at 600 °C. The sheet resistance (R_s) values increased with quenching time along with the free carrier concentration and mobility reduction (Figure 1). In order to discrete the respective influence of the

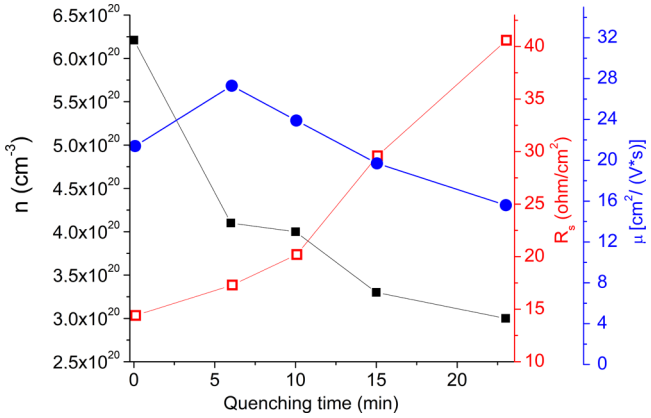

Figure 1. Sheet resistance (R_s), free carrier concentration (n), and Hall mobility (μ) as function of quenching time in air of the F:SnO_2 films.

free carrier concentration and mobility, a numerical calculation of the R_s values was performed (using the formulas $\rho = R_s.d$ and $\rho = 1/(n\mu e)$, where ρ is the resistivity and d is the layer thickness) by considering first a constant μ and then a constant n (Figure S1 in the Supporting Information). From there, it could be observed that the free carrier concentration modification had almost a double effect on R_s values as compared to mobility, meaning that the small oscillations in mobility contributed only slightly to the evolution in resistance.

Based on the overall diffractograms recorded for the nonquenched and quenched F:SnO_2 films (Figure 2a), we could not highlight any significant changes in the micro-

https://dx.doi.org/10.1021/acsomega.0c00589
ACS Omega 2020, 5, 14999−15006

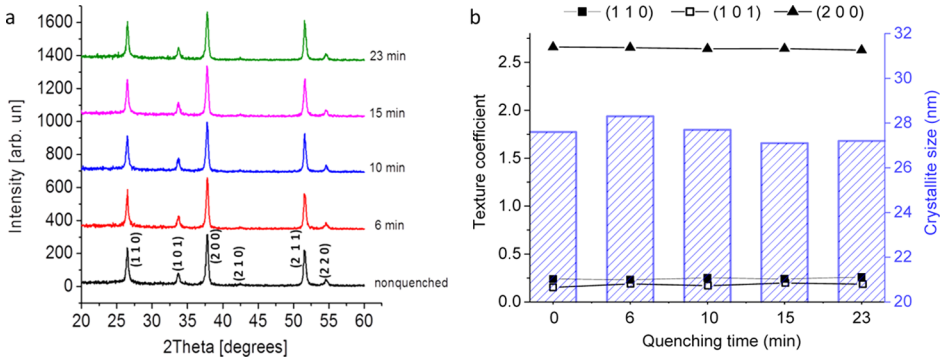

Figure 2. (a) X-ray diffraction (XRD) patterns and (b) average crystallite size (bars) and TC (triangles and squares) values calculated for the (110), (101), and (200) reflections for the F:SnO_2 films quenched in air at 670 °C for different times.

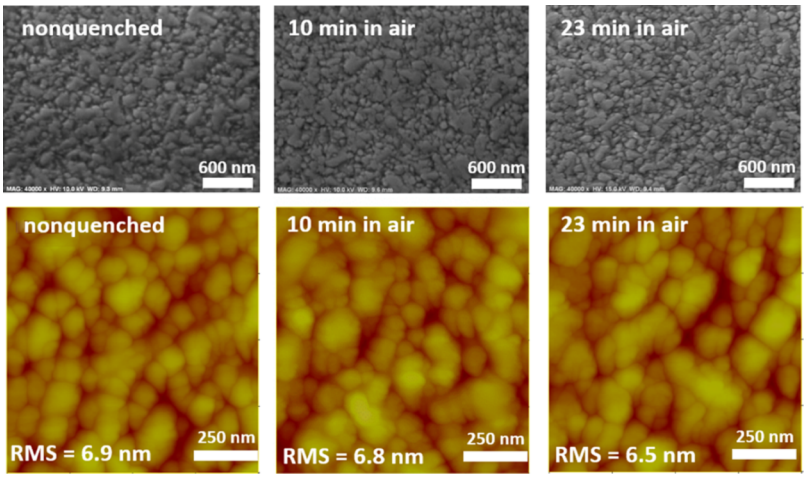

Figure 3. SEM (secondary electron mode, top row) and AFM (bottom row, root mean square roughness—rms—values are shown in the pictures) surface images of the F:SnO_2 films nonquenched (0 min) and quenched in air at 670 °C for 10 and 23 min. The standard deviation values for the rms measurements are ±0.1, ±0.3, and ±1.0 nm, respectively, whereas the instrument resolution is 1 nm.

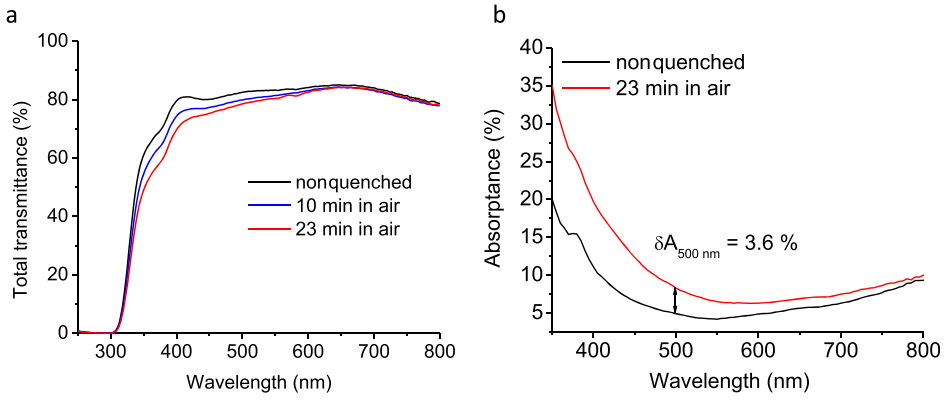

Figure 4. (a) Total transmittance and (b) absorptance spectra of the F:SnO_2 films nonquenched and quenched in air at 670 °C.

structure, that could explain the resistance drop. The cassiterite (SnO_2 rutile, ICCD PDF 04-003-0649) phase peaks were identified for both the nonquenched and quenched samples (Figure 2a). Crystallite size and texture coefficients (TC) were calculated for the (110), (101), and (200) reflections and were found to be almost invariable with quenching time (Figure 2b).

The F:SnO_2 films presented a (200) preferential orientation which did not vary much with quenching. As reported by Gao et al.,[26] using a Si_xC_yO barrier layer reinforces the (200) preferred orientation.

Scanning electron microscopy (SEM) (secondary electron mode) and atomic force microscopy (AFM) images (corresponding to a low and high magnification perspective, respectively) both showed that the surface topography was not affected by the quenching treatment (Figure 3).

Because neither structural nor morphological changes could explain the drop in conductivity, it was most likely that the layer composition had changed. This assumption was supported by the fact that the F:SnO_2 films visual aspect turned more and more yellowish with increasing quenching

https://dx.doi.org/10.1021/acsomega.0c00589
ACS Omega 2020, 5, 14999−15006

time (Figure S2 in the Supporting Information) as highlighted by the spectrophotometric measurements. A drop in transmittance was recorded (Figure 4a) and related to a change in absorptance (Figure 4b) and not in reflectance (reflectance curves of the F:SnO_2 films quenched for 23 min are shown in Figure S3 in the Supporting Information). The red shift of the absorptance curves with quenching in air was correlated with a slight decrease in the band gap (e.g., band gap extraction from the Tauc plots—represented in Figure S4—is detailed in the Supporting Information) and related to the creation of sub-band gap defects.[27] These defects act as absorption centers and should be mainly related to Na impurities rather than to oxygen vacancies as the preponderant passivation of vacancies would correspond to an increase in transmittance.

The $L^*a^*b^*$ chromaticity parameters [L^* is the lightness which varies from black (0) to white (100), a^* represents the variation from green (−) to red (+), whereas b* varies from blue (−) to yellow (+), and ΔE is the color difference calculated as $\Delta E = \mathrm{sqrt}[(\Delta L^*)^2 + (\Delta a^*)^2 + (\Delta b^*)^2$, with $\Delta E = 2.3$ corresponding to a just noticeable difference[28]] were further calculated from the transmittance spectra using a D65 illuminant, and values are shown in Table 1 for the nonquenched and 10 and 23 min quenched in air samples. The change in color toward a yellow tint after quenching was confirmed by the shift of the a^* and b^* parameters toward positive values (absorptance in the blue-violet region).

Table 1. $L^*a^*b^*$ Chromaticity Parameters and Color Difference (ΔE) for the Nonquenched and the F:SnO_2 Layers Quenched in Air and O_2 at 670 °C

sample	L^*	a^*	b^*	ΔE[a]
nonquenched	93.12	0.11	1.98	
10 min in air	92.33	0.49	2.95	1.31
23 min in air	91.90	0.54	3.92	2.33
23 min in O_2	91.45	0.65	3.60	2.39

[a] ΔE was calculated versus the nonquenched value.

Because the structural and morphological features of the layers did not change with quenching, it was reasonable to assume that the conductivity drop was related to the annihilation and/or creation of defects in the F:SnO_2 lattice. To that end, the hypothesis of oxygen vacancies passivation was further explored by quenching the F:SnO_2 films in an oxygen-rich (pure O_2) atmosphere.

The L^*, a^*, b^*, and ΔE parameters for the sample quenched in O_2 are also included in Table 1. It appeared that the F:SnO_2 layers quenched in O_2 and air turned yellowish nearly to the same extent at longer quenching times as confirmed by the similar ΔE values and almost identical transmittance curves (Figure S5 in the Supporting Information).

The "R_s," "n," and "μ" values for the F:SnO_2 films quenched for 23 min in air and O_2 with regard to the nonquenched film are summarized in Table 2. As expected, the free carrier concentration is smaller for the films annealed in O_2 compared to those annealed in air, but a more striking difference between quenching in air and in O_2 would have been expected if the oxygen vacancies passivation was the main reason for the conductivity drop.[29]

As previously concluded for the samples annealed in air, the crystalline phase and the preferred orientation did not change after quenching in O_2 and neither did the morphology (Figure S6a,b in the Supporting Information).

Table 2. Sheet Resistance (R_s), Free Carrier Concentration (n), and Hall Mobility (μ) Values for the Nonquenched and F:SnO_2 Layers Quenched in Air and O_2

sample	R_s (Ω cm^{-2})	n (cm^{-3})	μ (cm^2/(V s))
nonquenched	14.4 ± 0.1	6.2×10^{20} ± 0.5	21.4 ± 2.0
23 min in air	40.6 ± 0.1	3.0×10^{20} ± 0.3	15.5 ± 1.4
23 min in O_2	52.4 ± 0.3	2.0×10^{20} ± 0.3	17.6 ± 5.0

These results, along with the negligible change in the free carrier concentration, suggested that the variability in electrical properties was nested in some changes in composition, with a similar effect in both samples. Indeed, taking into consideration the free carrier concentration results for the samples quenched in air and O_2 for 23 min, the oxygen vacancies passivation could not be the main or sole mechanism behind such a behavior.

Other hypotheses reported in the literature involve Na diffusion from the glass bulk inside the F:SnO_2 structure[22,23] or the fluorine migration out of the F:SnO_2 structure during quenching causing the lattice expansion[15] or the creation of Sn vacancies along with the lattice contraction.[19] However, no factual proof of elements migration was given in these studies. It is important to mention that no shift in the XRD peaks position with quenching could be detected in our study.

The marked increase in resistance values after 10 min made us believe that the mechanism could occur in two steps, that is, for shorter quenching times (below 10 min), the carrier concentration would be mainly attributed to oxygen vacancy passivation, whereas for longer quenching times, Na diffusion from glass would have a higher impact in the scattering of the free charge carriers. The diffusing Na ions could lower the free carrier concentration by two mechanisms

(1) Reaction with the $F_O^\bullet$ donors (eq 5);
(2) Oxygen vacancies passivation with the formation of more Na_{Sn}^{3-} acceptor centers (eq 6).

$$Na_i^\bullet + F_O^\bullet \rightarrow Na - F + V_O^{\bullet\bullet} \quad (5)$$

$$Na_i^\bullet + V_O^x + 4e^- \rightarrow Na_{Sn}^{3-} \quad (6)$$

To support our hypothesis, XPS depth profiles were registered on the F:SnO_2 layers before and after quenching in air (10 and 23 min), as well as after quenching for 23 min in O_2. The purpose was to probe whether or not elements were diffusing from the glass or from the Si_xC_yO barrier layer. Prior to step-by-step XPS analysis, Ar^+ etching was performed. The etching rate was estimated to be 0.3 nm/s versus a SiO_2 layer.

The presence of carbon was detected at the surface because of ambient contamination, and its content reached 0 at. % after 60 nm etching (Figure 5a showing no carbon until 200 nm depth). The concentration of Sn decreased to 20 at. % after 720 s of etching time indicating a F:SnO_2 layer thickness of around 250 nm (theoretical etching rate: 0.3 nm/s for 720 s, meaning 216 nm).

Within the barrier layer (zone "Si_xC_yO," as shown in Figure 5a), the decrease in the C content and the increase in O after quenching in air and oxygen might indicate a slight oxidation of the barrier layer (SiO_x into SiO_2) with no consequence on the optical properties ($\Delta T = 0.55\%$ at 550 nm, Figure S7a in the Supporting Information).

However, a much more significant change in the transmittance of the barrier layer ($\Delta T = 3.7\%$ at 550 nm) was obtained when the Si_xC_yO barrier layer was quenched without

https://dx.doi.org/10.1021/acsomega.0c00589
ACS Omega 2020, 5, 14999−15006

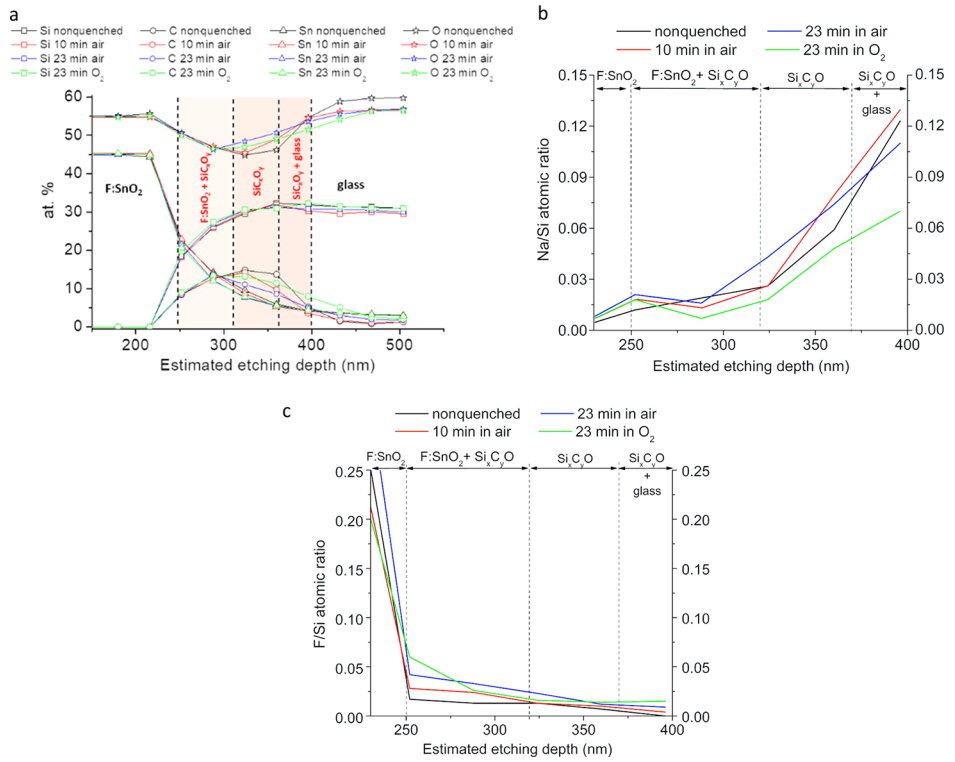

Figure 5. XPS depth profiles (atomic % extracted from the Si 2p, C 1s, Sn $3d_5$, and O 1s spectra) (a) and the evolution of the Na/Si (b) and F/Si (c) atomic ratios as function of the etching depth for the $F:SnO_2$ samples nonquenched ("0 min") and quenched in air and O_2 at 670 °C.

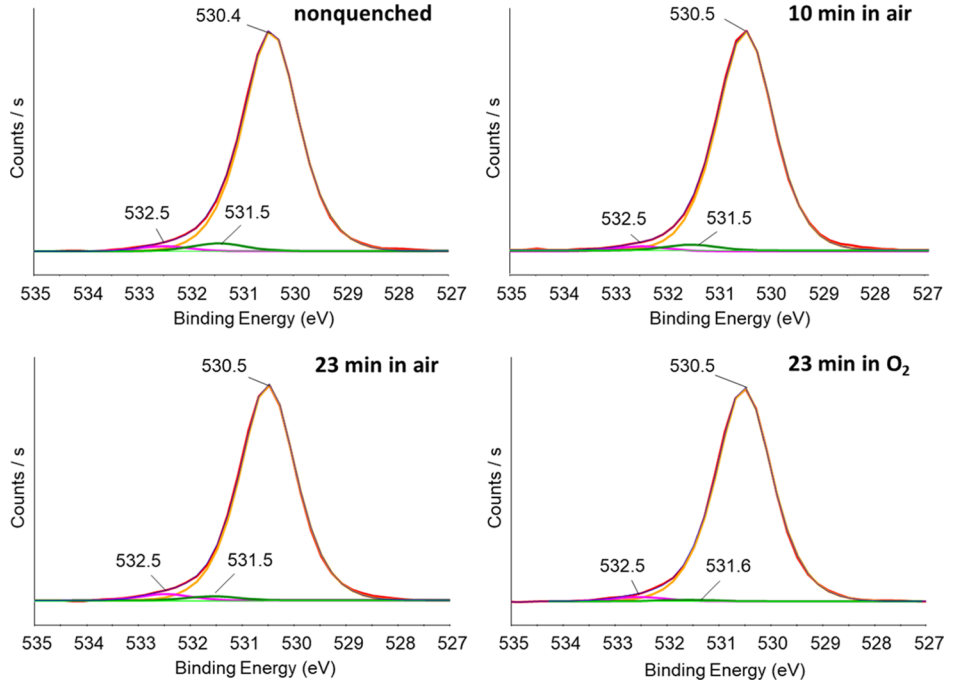

Figure 6. Fitted O 1s XPS spectra at 60 s etching level for the $F:SnO_2$ films nonquenched and quenched in air and O_2 at 670 °C.

the protection of the $F:SnO_2$ layer (previously removed by chemical etching) as the reflectance of the oxidized SiO_x was lower (Figure S7b,c in the Supporting Information). This proved that the change in color did not come from the barrier layer but could be originated in the upward (downward) elements diffusion into (from) the $F:SnO_2$ layer.

Interestingly, the XPS data would indicate the presence of a diffusion layer of more than 70 nm thickness at the interface between the $F:SnO_2$ and Si_xC_yO layers (labeled as "$F:SnO_2$ + Si_xC_yO" in Figure 5a). Such a diffusion layer was also identified by Wang et al.[25] by spectroscopic ellipsometry, having a thickness of around 13 nm. The C, O, and Si contents were quite constant over the 70 nm depth, thus defining the Si_xC_yO barrier layer thickness. Moreover, a second diffusion layer of around 30 nm thickness was more likely present at the interface with the glass bulk (labeled as "Si_xC_yO + glass" in

https://dx.doi.org/10.1021/acsomega.0c00589
ACS Omega 2020, 5, 14999−15006

Figure 5a) because the C content began to decrease and the O content increased markedly at this level of depth profiling.

For both the nonquenched and quenched F:SnO_2 layers, the XPS profiling indicated that Na could have diffused from the glass, through the barrier layer (Figure 5b), crossing the "F:SnO_2 + Si_xC_yO" diffusion layer. At the F:SnO_2/F:SnO_2 + Si_xC_yO interface, the Na content was higher for the quenched samples (Figure 5b) compared to the nonquenched one. This would correlate with the decrease of the Na levels in the proximity of the glass interface. Na could interfere in reducing the carrier concentration by reacting either with the fluorine donors or with the oxygen vacancies, as exemplified in eqs 5 and 6. Interestingly, the fluorine content at the F:SnO_2/F:SnO_2 + Si_xC_yO interface seemed to increase with increasing quenching time (Figure 5c). The F downward diffusion, which is nondetectable through XRD, would cancel the positive effect of doping leading to conductivity drop. The O_2 inward diffusion from the atmosphere seemed to interfere with Na diffusion as for the sample quenched in O_2 the Na levels in the "F:SnO_2 + Si_xC_yO" diffusion layer were lower compared to the sample quenched in air.

Fitting of the O 1s XPS spectra corresponding to the F:SnO_2 near surface (60 s etching time) could be proposed with three contributions (Figure 6): one at around 530.5 eV corresponding to O^{2-} in the SnO_2 lattice, another one around 531.5 eV attributed to oxygen vacancies in SnO_2,[30] and the third at around 532.5 eV corresponding to chemisorbed −OH.[31]

Concerning the main O^{2-} component, there was practically no change in the O 1s peak full width at half-maximum (fwhm) value (i.e., 1.32 eV) for the F:SnO_2 layers before and after quenching in air or O_2. This was consistent with the XRD results which showed no change in the layer crystallinity. The V_O^x proportion in the O1s peak was calculated, and the V_O^x/O^{2-} ("531.5/530.5 eV") component ratios were 0.032, 0.025, 0.017, and 0.007 for the nonquenched, 10, 23 min in air, and 23 min in O_2, respectively. These proportions were quite small because of the high temperature deposition conditions which stabilized the F:SnO_2 layer toward quenching. Higher variations in the oxygen vacancy peak were reported for the layers prepared by chemical/low-temperature methods.[22,29] However, two main trends could be drawn, that is, the oxygen vacancy content decreased with quenching time and in the oxygen-rich atmosphere, the oxygen vacancies passivation was emphasized. Nevertheless, the small difference in the free carrier concentration and optical properties between the layers annealed in air and O_2 pointed to the fact that, indeed, the differences in the V_O^x/O^{2-} proportion were negligible. Implicitly, Na and F diffusion should mainly contribute to the conductivity drop for longer quenching times, with a mitigated effect for Na in the oxygen-rich atmosphere.

3. CONCLUSIONS

The influence of quenching on the opto-electronic properties of the F:SnO_2 layers deposited at high temperature by APCVD on the Si_xC_yO-coated glass was investigated with regard to morphology, structural, and composition changes.

The structure and morphology of the studied F:SnO_2 layers were found invariant to quenching in air or O_2 as the samples microstructure was practically fringed through deposition at high temperatures.

Moreover, the visible transmittance of the F:SnO_2 layers was markedly affected by tempering as Na impurities act as absorption and electron recombination centers. Changes in the optical properties of the barrier layer were excluded through spectrophotometric measurements.

XPS in-depth profiling seemed to indicate the existence of two diffusion layers at the F:SnO_2/Si_xC_yO and Si_xC_yO/glass interfaces, already present before quenching.

The layers conductivity decreased with quenching time in air because of free carrier concentration reduction. Na upward diffusion from the glass into the F:SnO_2 layer and F downward diffusion from the F:SnO_2 layer were also proposed through XPS. Along with the elements diffusion, the oxygen vacancy diminution was found responsible for the conductivity drop for shorter quenching times (<10 min). For longer quenching times (>20 min), it seemed that Na and F diffusion mainly contributed to free charge carrier diminution. A less marked difference in the free carrier concentration and transmittance was observed for the sample quenched in O_2 compared to air and related to a possible moderation in the Na diffusion by incoming oxygen.

For a 300 nm thick F:SnO_2 layer, the contribution of Na diffusion to the free charge carrier scattering could be minimized by keeping the quenching periods within 10 min.

This study emphasizes the importance and the complicity between the two factors that would contribute to the conductivity loss in highly crystalline APCVD-prepared F:SnO_2 layers subjected to quenching, that is, the oxygen vacancy passivation and the diffusion of impurities inside and outside the F:SnO_2 layer.

4. EXPERIMENTAL AND CALCULATIONS

4.1. F:SnO_2 Deposition. The F:SnO_2 films (320 nm thick, 14 Ω/sq) were deposited by APCVD at 600 °C on the glass coated with a Si_xC_yO layer. Monobutyl tin trichloride and HF were used as tin and fluorine precursors, respectively, and air was used as carrier gas. After deposition, samples were polished for optical properties optimization.

4.2. Samples Cleaning and Quenching. After being cleaned with the neutral pH surfactant and rinsed consecutively in deionized water and ethanol in the ultrasonic bath for 10 min followed by drying under compressed air stream, the glass samples were quenched.

For quenching in air, the samples were placed in an open-air furnace once the temperature was reached (670 °C) and removed after a defined period (6, 10, 15, and 23 min). The quenching treatment in the O_2 atmosphere was performed in a tubular furnace for 23 min at the same temperature. The quenching times and temperatures were selected based on the literature reports.[21,23−25]

4.3. Opto-Electronic Characterization. The electrical characterization (sheet resistance, carrier concentration, and Hall mobility) was performed using a PhysTechRH 2035 system in Van der Pauw 4-points configuration (Sn contacts of 1.5 mm diameter, placed at 12 mm distance of each other in a square perimeter configuration). For the Hall effect measurements, a fixed magnetic field (0.43 T) was used.

Optical characterizations were realized using the Shimadzu UV3600 Plus UV−vis−NIR ($BaSO_4$ integrating sphere, Ø = 15 cm) spectrophotometer, and the Panorama software was used for the chromaticity parameter calculation.

4.4. Microstructural Characterization. XRD structural characterization was performed on a Bruker D8 Discovery diffractometer (grazing incidence, Cu Kα radiation, α = 0.154 nm, 20° < 2θ < 60°, step width 0.04 and 2° incidence angle).

https://dx.doi.org/10.1021/acsomega.0c00589
ACS Omega 2020, 5, 14999−15006

The crystallite size was calculated for the (110), (101), and (200) reflections by using the Scherrer equation

$$D = \frac{K\lambda}{\beta \cos\theta} \quad (7)$$

where K is a dimensionless shape factor and typically equals 0.9, λ is the wavelength of the incident Cu Kα radiation (1.5418 Å), β is the line broadening at fwhm of the diffraction peak (measured in radians), and θ is the Bragg angle.

The TC were calculated for the (110), (101), and (200) main peaks, using the formula below

$$TC_{(hkl)} = \frac{\left(\frac{I_{(hkl)}}{I_{0(hkl)}}\right)}{\frac{1}{2}\sum_{i=1}^{2}\left(\frac{I_{(hkl)}}{I_{0(hkl)}}\right)} \quad (8)$$

In the formula, $I_{(hkl)}$ represents the net area of the peak (110), (101), or (200), and $I_{0(hkl)}$ is the net area of the same peaks corresponding to a reference sample which presents random orientation. The reference sample was SnO_2 powder (Sigma-Aldrich, $p \geq 99.9\%$, <100 nm particle size) which was measured in the same conditions as the sample.

AFM (Digital Instrument Nanoscope III microscope from Veeco) measurements were performed in a tapping mode with a super sharp (NSG30_SS/10 from NT-MDT, tip diameter < 5 nm) improved super cone probe.

SEM characterizations were performed with an ESEM-FEG XL30 FEI instrument operated at 15 kV (secondary electron mode).

4.5. Chemical Characterization. A Thermo Fisher Scientific K-Alpha spectrometer (monochromatized Al Kα source, $h\nu$ = 1486.6 eV, spot size 200 μm) was used for XPS depth profiling of the F:SnO_2-covered glass samples. All binding energy values were determined with respect to the C1s maximum peak at 284.9 eV. Etching was performed using an Ar^+ ion gun at 500 eV (20 levels in total with high-resolution spectra recorded alternately with sputtering time). Quantification and peak fitting were achieved by using the AVANTAGE software (Thermo Fisher Scientific).

■ ASSOCIATED CONTENT

Supporting Information

The Supporting Information is available free of charge at https://pubs.acs.org/doi/10.1021/acsomega.0c00589.

Numerical simulations, pictures of the samples before and after quenching, reflectance and/or transmittance spectra of the F:SnO_2 and Si_xC_yO barrier layers before and after quenching in air/O_2, band gap extraction, XRD, SEM, and AFM results of the sample quenched in O_2 atmosphere (PDF)

■ AUTHOR INFORMATION

Corresponding Authors

Laura Maria Manceriu − *UR CESAM, GREEnMat, University of Liège, B-4000 Liège, Belgium;* orcid.org/0000-0002-3990-7916; Phone: +32 (0)4 366 3533; Email: laura.manceriu@uliege.be; Fax: +32 (0)4 366 4747

Rudi Cloots − *UR CESAM, GREEnMat, University of Liège, B-4000 Liège, Belgium;* orcid.org/0000-0002-2648-0407; Phone: +32 (0)4 366 3436; Email: rcloots@uliege.be; Fax: +32 (0)4 366 4747

Authors

Anthony Maho − *UR CESAM, GREEnMat, University of Liège, B-4000 Liège, Belgium;* orcid.org/0000-0002-3813-6240

Christine Labrugere − *CNRS, Université de Bordeaux, PLACAMAT UMS 3626, F-33600 Pessac, France*

Eric Tixhon − *AGC Glass Europe S.A, Technovation Centre, B-6041 Gosselies, Belgium*

Audrey Schrijnemakers − *UR CESAM, GREEnMat, University of Liège, B-4000 Liège, Belgium;* orcid.org/0000-0003-3276-1798

Aline Rougier − *CNRS, Université de Bordeaux, Bordeaux INP, ICMCB, UMR 5026, F-33600 Pessac, France;* orcid.org/0000-0002-1340-734X

Pierre Colson − *UR CESAM, GREEnMat, University of Liège, B-4000 Liège, Belgium*

Complete contact information is available at: https://pubs.acs.org/10.1021/acsomega.0c00589

Notes

The authors declare no competing financial interest.

■ ACKNOWLEDGMENTS

The authors are grateful to the Walloon Region and AGC Flatglass for financial support (project no. 7428).

■ ADDITIONAL NOTE

[a]In these four equations, the Kroger−Vink notation is used: V_{Sn}^{4-} is a tin vacancy with 4- effective charge because of the missing four positive charges coming from Sn^{4+}; $F_O^{\bullet}$ means that the F atom has substituted an oxygen atom in the lattice, and the positive charge comes from the fact that a negative charge was removed from the normal lattice; O_i'' is an oxygen interstitial with 2- effective charge because two supplementary negative charges are inserted into the network; O_0^x and F_0^x are the oxygen and fluorine in their normal place in the lattice; V_O^x and $V_O^{\bullet\bullet}$ are the neutrally and double positively charged oxygen vacancies, respectively.

■ REFERENCES

(1) Granqvist, C. G.; Hultåker, A. Transparent and conducting ITO films: new developments and applications. *Thin Solid Films* **2002**, *411*, 1−5.

(2) Gubbala, S.; Chakrapani, V.; Kumar, V.; Sunkara, M. K. Band-Edge Engineered Hybrid Structures for Dye-Sensitized Solar Cells Based on SnO_2 Nanowires. *Adv. Funct. Mater.* **2008**, *18*, 2411−2418.

(3) Noor, N.; Parkin, I. P. Enhanced transparent-conducting fluorine-doped tin oxide films formed by Aerosol-Assisted Chemical Vapour Deposition. *J. Mater. Chem. C* **2013**, *1*, 984−996.

(4) Snaith, H. J.; Ducati, C. SnO_2-Based Dye-Sensitized Hybrid Solar Cells Exhibiting Near Unity Absorbed Photon-to-Electron Conversion Efficiency. *Nano Lett.* **2010**, *10*, 1259−1265.

(5) Chae, G. S. A modified transparent conducting oxide for flat panel displays only. *J. Appl. Phys.* **2001**, *40*, 1282−1286.

(6) Bârsan, N. Conduction models in gas-sensing SnO_2 layers: grain-size effects and ambient atmosphere influence. *Sens. Actuators, B* **1994**, *17*, 241−246.

(7) Lampert, C. M. Heat mirror coatings for energy conserving windows. *Sol. Energy Mater. Sol. Cells* **1981**, *6*, 1−41.

(8) Fonstad, C. G.; Rediker, R. H. Electrical properties of High-quality stannic oxide crystals. *J. Appl. Phys.* **1971**, *42*, 2911−2918.

(9) Zhang, G.; Xie, C.; Zhang, S.; Yang, L.; Xiong, Y.; Zeng, D. Temperature- and Atmosphere-Dependent Defect Chemistry Model of SnO2Nanocrystalline Film. *J. Am. Ceram. Soc* **2014**, *97*, 2091−2098.

(10) Rottkay, K.; Rubin, M. Optical Indices of Pyrolytic Tin-Oxide Glass. *MRS Online Proc. Libr.* **1996**, *426*, 449.
(11) Gordon, R. G. Criteria for Choosing Transparent Conductors. *MRS Bull.* **2000**, *25*, 52−57.
(12) Remes, Z.; Vanecek, M.; Yates, H. M.; Evans, P.; Sheel, D. W. Optical properties of SnO_2:F films deposited by atmospheric pressure CVD. *Thin Solid Films* **2009**, *517*, 6287−6289.
(13) https://www.vitroglazings.com/products/special-applications/heat-treated-glass, consulted the 13.06.2020.
(14) Paz, Y.; Heller, A. Photo-oxidatively self-cleaning transparent titanium dioxide films on soda lime glass: the deleterious effect of sodium contamination and its prevention. *J. Mater. Res.* **1997**, *12*, 2759−2766.
(15) Gao, Q.; Li, M.; Li, X.; Liu, Y.; Song, C. L.; Wang, J. X.; Liu, Q. Y.; Liu, J. B.; Han, G. R. Microstructural and functional stability of large-scale SnO_2:F thin film with micro-nano structure. *J. Alloy. Comp.* **2013**, *550*, 144−149.
(16) Ikhmayies, S. J. The influence of annealing on the optical properties of spray-deposited SnO_2:F thin films. *Int. J. Hydrog. Energy* **2016**, *41*, 12626−12633.
(17) Mehraj, S.; Ansari, M. S.; Alimuddin, A. Annealed SnO_2 thin films: Structural, electrical and their magnetic properties. *Thin Solid Films* **2015**, *589*, 57−65.
(18) Akkad, F. E.; Joseph, S. Physicochemical characterization of point defects in fluorine doped tin oxide films. *J. Appl. Phys.* **2012**, *112*, 023501.
(19) Akkad, F. E.; Paulose, T. A. P. Optical transitions and point defects in F:SnO_2 films: Effect of annealing. *Appl. Surf. Sci.* **2014**, *295*, 8−17.
(20) Gao, Q.; Liu, Q.; Li, M.; Li, X.; Liu, Y.; Song, C.; Wang, J.; Liu, J.; Shen, G.; Han, G. Effect of glass tempering on microstructure and functional properties of SnO_2:F thin film prepared by atmosphere pressure chemical vapor deposition. *Thin Solid Films* **2013**, *544*, 357−361.
(21) Wang, K.; Cheng, B.; Wu, B.; Defranoux, C.; Basa, P.; Song, C.; Han, G.; Liu, Y. Study of annealing effects upon the optical and electrical properties of SnO_2:F/Si_xC_yO low emissivity coatings by spectroscopic ellipsometry. *Thin Solid Films* **2014**, *571*, 720−726.
(22) Wang, R. X.; Beling, C. D.; Fung, S.; Djurišić, A. B.; Ling, C. C.; Li, S. Influence of gaseous annealing environment on the properties of indium-tin-oxide thin films. *J. Appl. Phys.* **2005**, *97*, 033504.
(23) Yang, J.; Liu, W.; Dong, L.; Li, Y.; Li, C.; Zhao, H. Studies on the structural and electrical properties of F-doped SnO_2 film prepared by APCVD. *Appl. Surf. Sci.* **2011**, *257*, 10499−10502.
(24) Yang, J. K.; Zhao, H. L.; Li, J.; Zhao, L. P.; Chen, J. J.; Yu, B. Structural and optical properties and photoluminescence mechanism of fluorine-doped SnO_2 films during the annealing process. *Acta. Mater.* **2014**, *62*, 156−161.
(25) Wang, K.; Hua, Y.; Wang, J.; Song, C.; Jia, S.; Han, G.; Liu, Y. Optical and structural characterization of SnO_2:F/Si_xC_yO tandem thin films by spectroscopic ellipsometry. *Thin Solid Films* **2013**, *540*, 84−91.
(26) Gao, Q.; Li, M.; Liu, Q.; Wang, Y.; Li, X.; Wei, X.; Song, C.; Wang, J.; Liu, J.; Shen, G.; Han, G. Enhanced preferential orientation and electrical property of fluorine-doped SnO_2 thin films via barrier layer. *Mater. Lett.* **2014**, *122*, 143−146.
(27) Rucavado, E.; Graužinytė, M.; Flores-Livas, J. A.; Jeangros, Q.; Landucci, F.; Lee, Y.; Koida, T.; Goedecker, S.; Hessler-Wyser, A.; Ballif, C.; Morales-Masis, M. New Route for "Cold-Passivation" of Defects in Tin-Based Oxides. *J. Phys. Chem. C* **2018**, *122*, 17612−17620.
(28) Sharma, G. *Digital Color Imaging Handbook*, 2013; Boca Raton, F. L., Ed.; CRC Press Taylor & Francis Group: New York, 2003; p 31.
(29) Jeng, J.-S. The influence of annealing atmosphere on the material properties of sol−gel derived SnO_2:Sb films before and after annealing. *Appl. Surf. Sci.* **2012**, *258*, 5981−5986.
(30) Clatot, J.; Campet, G.; Zeinert, A.; Labrugère, C.; Nistor, M.; Rougier, A. Low temperature Si doped ZnO thin films for transparent conducting oxides. *Sol. Energy Mater. Sol.* **2011**, *95*, 2357−2362.
(31) Amanullah, F. M.; Pratap, K. J.; Hari Babu, V. Compositional analysis and depth profile studies on undoped and doped tin oxide films prepared by spray technique. *Mater. Sci. Eng., B* **1998**, *52*, 93−98.

https://dx.doi.org/10.1021/acsomega.0c00589
ACS Omega 2020, 5, 14999−15006